analytical chemistry

pubs.acs.org/ac Article

Near-Infrared Light-Initiated Photoelectrochemical Biosensor Based on Upconversion Nanorods for Immobilization-Free miRNA Detection with Double Signal Amplification

Mengjiao Hao, Pei Miao, Yan Wang, Wenshou Wang, Shenguang Ge, Xinyan Yu, Xiao-Xiao Hu, Biyan Ding, Jing Zhang,* and Mei Yan*

Cite This: *Anal. Chem.* 2021, 93, 11251−11258 Read Online

ACCESS | Metrics & More | Article Recommendations | Supporting Information

ABSTRACT: Photoelectrochemical (PEC) sensors are relatively new sensing platforms with high detection sensitivity and low cost. However, the current PEC biosensors dependent on ultraviolet or visible light as the exciting resource cause injuries to biological samples and systems, which restrains the applications in complicated matrixes. Herein, a near-infrared light (NIR)-initiated PEC biosensor based on $NaYF_4$:Yb,Tm@$NaYF_4$@TiO_2@CdS (csUCNRs@TiO_2@CdS) was constructed for sensitive detection of acute myocardial infarction (AMI)-related miRNA-133a in an immobilization-free format coupled with a hybridization chain reaction and a redox circle signal amplification strategy. A low-energy 980 nm NIR incident laser was converted to 300−480 nm light to excite the adjacent TiO_2@CdS photosensitive shell to generate photocurrent by $NaYF_4$:Yb,Tm@$NaYF_4$ upconversion nanorods. Also, magnetic beads were employed for the homogeneous determination of target miRNA-133a to reduce the recognition steric hindrance and improve the detection sensitivity. The photocurrent response was positively correlated with the level of ascorbic acid as the energy donor to consume photoacoustic holes produced on the surface of csUCNRs@TiO_2@CdS, which was generated by alkaline phosphatase catalyzation and regenerated by tris(2-carboxyethyl) phosphine reduction upon the appearance of miRNA-133a. Exerting a NIR-light-driven and immobilization-free strategy, the as-constructed biosensor displayed linearly sensitive and selective determination of miRNA-133a with a detection limit of 36.12 aM. More significantly, the assay method provided a new concept of the PEC sensing strategy driven by NIR light to detect diverse biomarkers with pronounced sensitivity, light stability, and low photodamage.

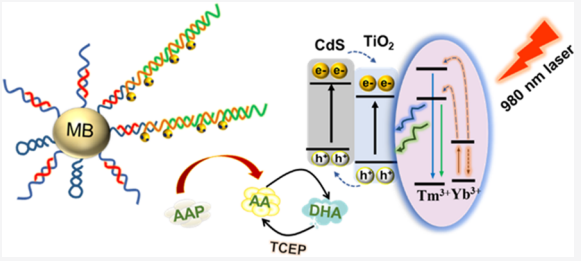

INTRODUCTION

MiRNA-133a as a kind of single-stranded microRNA (miRNA) with approximately 20 nucleotides[1,2] plays an essential part in the regulation of cardiac proliferation, differentiation, and apoptosis based on the fact that it can reduce ventricular remodeling and improve cardiac function after stress load.[3,4] MiRNA-133a is a promising candidate for acute myocardial infarction (AMI), monitoring for the immediate level fluctuations due to cardiac abnormal situations.[5] Nevertheless, the low concentration and short and similar sequences of endogenous miRNA-133a in a biological environment hinder the sensitive and practical monitoring of AMI in time.[6] Therefore, a highly sensitive and biocompatible detection method for miRNA-133a is desirable and valuable for early diagnosis of AMI.

Photoelectrochemical (PEC) sensors are relatively new sensing platforms that implement the separation of the incident light source and detection signal,[7,8] resulting in pronounced detection sensitivity as compared to other mothods.[9,10] Moreover, PEC sensors are superior in the detection field due to the low cost, simple equipment, and easy miniaturization.[11] However, the current PEC biosensors employing ultraviolet (UV) or visible (vis) laser with high energy as the excitation source still have great challenges to biological signal species determination due to the strong light damage to samples and systems and biological interferences.[12,13] In addition, the conventional immobilized methodology that most PEC biosensors use suffers from insufficient sensitivity and repeatability, low reaction rate, and target-recognition efficiency due to the steric hindrance effect on the surface of the modified electrode.[14−16] Favorably, upconversion nanoparticles (UCNPs) can absorb NIR light sequentially and emit UV/vis light due to the ladder-like energy levels of Ln^{3+} ions,[17−19] presenting a series of merits including high chemical and optical stability and low phototoxicity owing to the utilization of the NIR light source.[20−24] UCNPs exhibit

Received: May 23, 2021
Accepted: July 29, 2021
Published: August 9, 2021

https://doi.org/10.1021/acs.analchem.1c02160
Anal. Chem. 2021, 93, 11251−11258

Scheme 1. (A) Immobilization-Free Detection of miRNA-133a Based on Magnetic Beads with HCR Amplification; (B) Synthetic Process of csUCNRs@TiO_2@CdS Photoactive Material; and (C) Mechanism of Photocurrent Enhancement Based on the Generated AA in (A) and Photoactive Material in (B) under 980 nm NIR Light with a Redox Circle Amplification

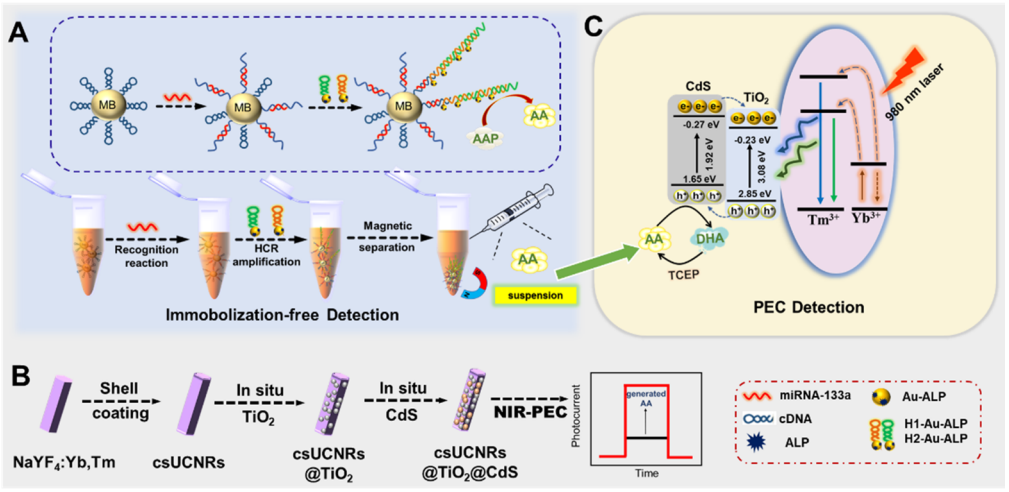

great competitiveness in PEC sensing fields and photocatalysis,[25] biological imaging,[26−28] optical encoding, and photoactive therapy.[29,30] More inspiringly, it is mainly in the solid host lattice that the luminescence process of Ln^{3+}-doped UCNPs is conducted, which effectively precludes the effects of the external environment (pH, humidity, or buffer).[31] Thus, the utilization of UCNPs in PEC biosensors is promising for biodetection, and the photocurrent response will be enhanced if an immobilization-free strategy is also employed.

UCNPs-based PEC biosensors composed of UCNPs and semiconductors with matched energy bands integrate both the merits of UCNPs and PEC assays such as low light injury to biological samples and high sensitivity,[32,33] which can be a breakthrough point for molecular signaling detection in complex biological environments.[34,35] Simultaneously, the introduction of a nonimmobilization strategy,[36−38] i.e., recognition and digestion processes are carried out in solution, can further help to obtain guaranteed sensitivity.[39,40] A UCNRs-based PEC sensing platform was developed and realized the sensitive determination of CEA by means of magnetic beads (MB) under NIR light irradiation.[41] After that, a $NaYF_4$:Yb,Tm@ZnO upconverter was constructed to detect CEA antigens using a homemade 3D-printed device.[32] Moreover, a diffusivity-mediated PEC biosensor was developed and the recognition and digestion process were carried out in solution with a low detection limit of miRNA-155.[42] Based on the above situations, the UCNP-based PEC biosensing platforms driven by a NIR light source in an immobilization-free detection manner showed enormous potential and advantages in the field of biomarker determination, even in complicated biological matrixes.

Herein, a NIR-initiated PEC biosensor on the basis of core−shell−shell structured $NaYF_4$: Yb, Tm@$NaYF_4$@TiO_2@CdS was proposed for the highly sensitive determination of miRNA-133a in an immobilization-free manner with double signal amplification. The core−shell $NaYF_4$:Yb, Tm@$NaYF_4$ upconversion nanorods (denoted as csUCNRs) were used as the energy donor to emit UV/vis light to excite the TiO_2@CdS shell and generate photocurrent under 980 nm excitation. The doubly amplified signal of miRNA-133a was acquired through a hybridization chain reaction (HCR) and redox circle strategy. Upon recognition between miRNA-133a and cDNA in solution, the 3′ end of the hairpin structure-opened cDNA triggered the HCR and alkaline phosphatase (ALP) in the product, catalyzing ascorbic acid 2-phosphate (AAP) to ascorbic acid (AA) to enhance photocurrent. Thereafter, the oxidation product dehydroascorbic acid (DHA) was in turn reduced by tris-(2-carboxyethyl) phosphine (TCEP) in the detection pull to AA through a redox circle process for further photocurrent amplification. This NIR-initiated biosensor provided a new strategy for the determination of low-abundance miRNAs in biological samples.

EXPERIMENTAL SECTION

Preparation of Core−Shell−Shell Structured $NaYF_4$:Yb,Tm@$NaYF_4$@TiO_2 Sensitive Material (csUCNRs@TiO_2@CdS). The EDTA-stabilized $NaYF_4$:Yb,Tm core was initially fabricated through an improved solvothermal method.[43] To obtain the core−shell csUCNRs, $RECl_3$ (RE: Y, Yb, Tm) solution was used and the synthesis process was the same as that for the core described in detail in the Supporting Information. Then, the TiO_2 layer was directly introduced into the $NaYF_4$:Yb,Tm surface with the help of PVP as the bridging agent through a mature method with minor modification.[44] Finally, to synthesize the csUCNRs@TiO_2@CdS hybrid materials, thioacetamide (0.038 g, 0.50 mmol) was dissolved in chromium nitrate solution (0.39 mmol, 40 mL) under stirring followed by the addition of csUCNRs@TiO_2 (0.15 g, 0.53 mmol) nanocomposites. Then, the resulting products were maintained at 160 °C for 2 h. The hybrid material was processed as above.

Synthesis of cDNA-Coupled Carboxylated Magnetic Beads (cDNA-MB). The amino-terminated cDNA was conjugated with previously purchased carboxylated magnetic beads via a carbodiimide coupling reaction, and the detailed experimental steps are described in the Supporting Information.

Preparation of ALP-Au-H1 and ALP-Au-H2 Conjugates. First, the Au nanoparticles was synthesized through the classical sodium citrate reduction.[45] Before the conjugation between Au and the H1 probe and ALP, a solution of K_2CO_3 (0.1 M) was utilized to adjust the pH of the Au nanoparticle

https://doi.org/10.1021/acs.analchem.1c02160
Anal. Chem. 2021, 93, 11251−11258

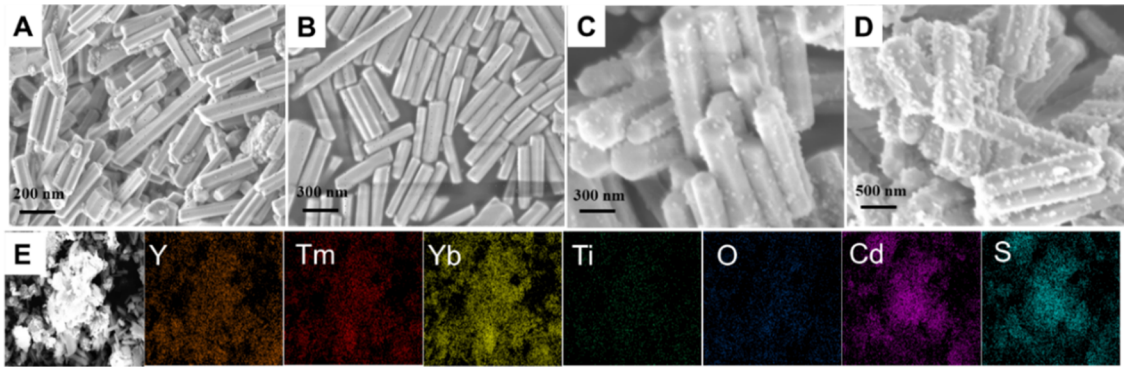

Figure 1. SEM images of (A) $NaYF_4$:Yb,Tm, (B) csUCNRs, (C) csUCNRs@TiO_2, (D) csUCNRs@TiO_2@CdS; (E) SEM elemental mapping of csUCNRs@TiO_2@CdS.

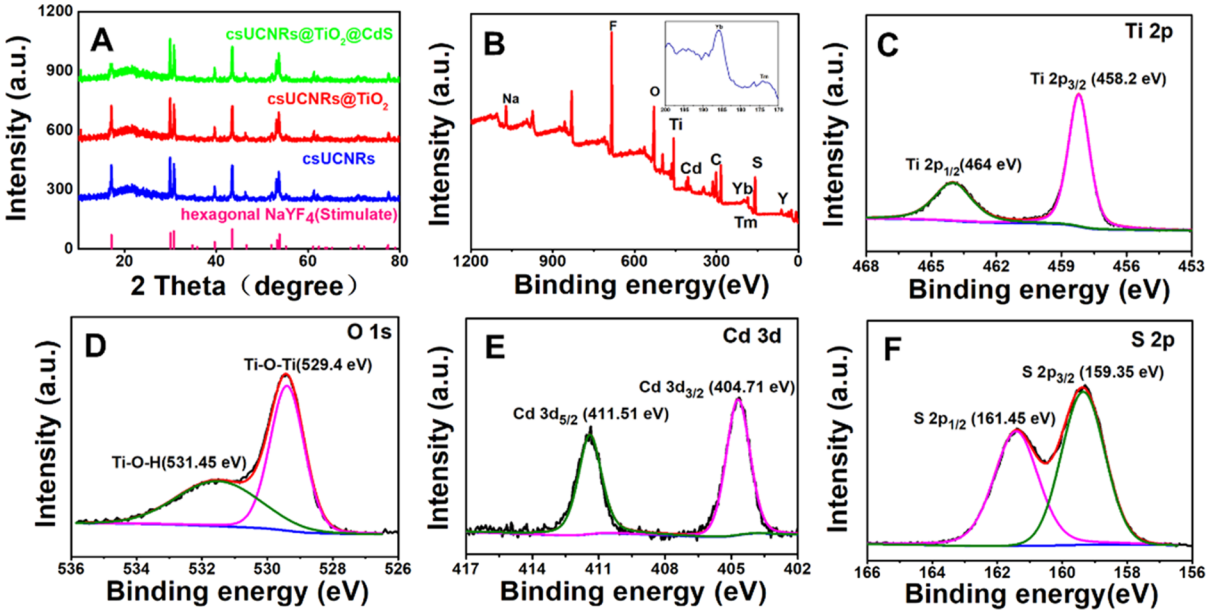

Figure 2. (A) XRD patterns of csUCNRs, csUCNRs@TiO_2, and csUCNRs@TiO_2@CdS; (B) full XPS spectrum of csUCNRs@TiO_2@CdS and corresponding high-resolution spectrum of (C) Ti 2p, (D) O 1s, (E) Cd 3d, and (F) S 2p orbitals.

suspension to 8.2.[46] In addition, the H1 probe (100 μL, 1.0 μM in TM buffer) and ALP solution (200 μL, 0.8 mg/mL) were thrown into the aforementioned 10.0 mL of Au NP suspension and reacted for 2.5 h at room temperture. Then, the precipitate was washed several times with TM buffer. Finally, the product was pipetted into 200 μL of TM buffer. ALP-Au-H2 was fabricated in the same method.

Fabrication of the NIR-Initiated PEC Biosensor and Photocurrent Measurement. The target miRNA-133a (20 μL) with various concentrations and cDNA-MB (60 μL, 5.0 mg/mL) were scattered into TE buffer (50 μL) and incubated for 2.5 h at 37 °C. The suspension was rinsed with freshly prepared PBS buffer magnetically. After that, the collected product was redispersed into 50 μL of TM buffer containing ALP-Au-H1 and ALP-Au-H2 conjugates (1.0 μM) and AAP (2.0 mM) and reacted at 37 °C for 3 h. After that, the supernatant containing generated AA after magnetic separation was dropped into the PEC detection pull. Prior to the detection, indium tin oxide (ITO) glasses were initially washed ultrasonically in acetone, ultrapure water, ethyl alcohol successively. Then, csUCNRs@TiO_2@CdS hybrid material solution (10 μL, 2 mg/mL) mixing with Nafion solution (0.1 μL) was casted on ITO electrode as the working electrode and dried under a NIR lamp.

All PEC detections were performed in a homemade PEC detection pull. The photocurrent on behalf of the miRNA concentration was recorded using an $i-t$ curve at 0 V.

RESULTS AND DISCUSSION

Characterization of csUCNRs@TiO_2@CdS. The target-responsive photocurrent acquirement consisted of two main procedures: (i) the recognition of target miRNA-133a homogeneously in solution with the aid of MBs and (ii) the photocurrent measurement in the PEC detection pull depend on the level of generated AA in the first step (Scheme1). First, miRNA-133a was hybridized by hairpin-structure cDNA attaching on magnetic beads through sequence-specific base pairing accompanied by the opening of cDNA. Also, the end of cDNA subsequently triggered the hybridization chain reaction (HCR) between H1 and H2 for signal amplification. The H1 and H2 probes were both modified with gold nanoparticles at the terminal of the chain through a Au−S bond. Furthermore, the AAP in solution was catalyzed by ALP connected to gold nanoparticles to AA acting as electron donors. After that, the

https://doi.org/10.1021/acs.analchem.1c02160
Anal. Chem. 2021, 93, 11251−11258

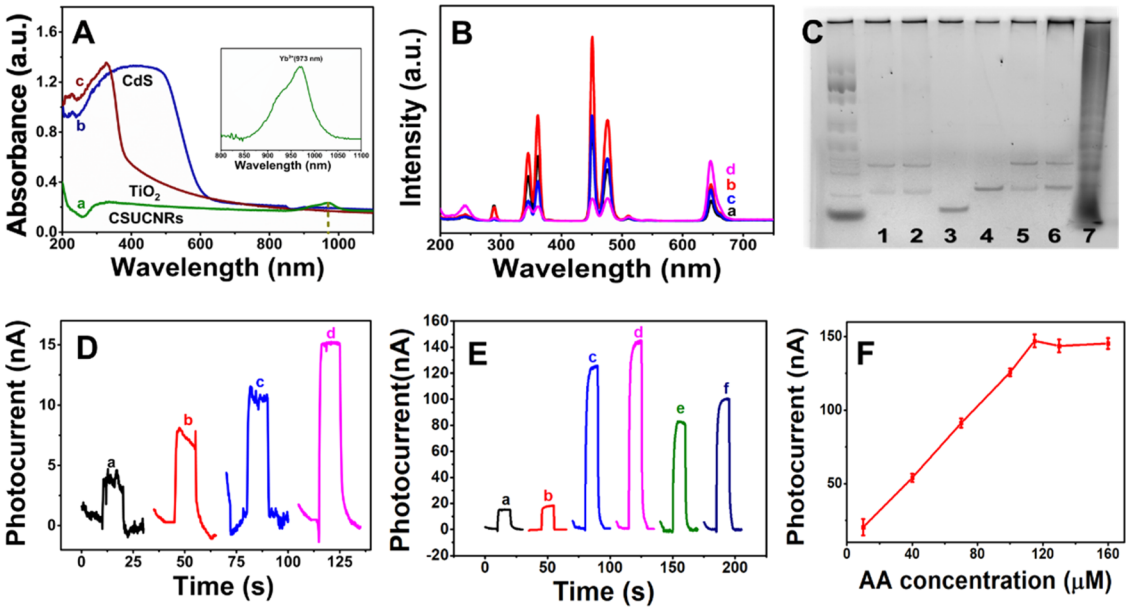

Figure 3. (A) UV−vis absorption spectra of (a) csUCNRs, (b) CdS, and (c) TiO_2 (insets: the amplified spectra of csUCNRs); (B) fluorescence emission spectrum of (a) $NaYF_4$:Yb, Tm, (b) csUCNRs, (c) csUCNRs@TiO_2, and (d) csUCNRs@TiO_2@CdS under a 980 nm laser; (C) native PAGE image of HCR (lane 0, DNA marker:25 bp; lane 1, H1; lane 2, H2; lane 3, miRNA-133a; lane 4, cDNA; lane 5, H1 + H2; lane 6, H1 + H2 + cDNA; lane 7, target miRNA-133a + H1 + H2 + cDNA); (D) photocurrents of photoactive material-modified ITO electrodes under 980 nm excitation (a−d correspond to those in Figure 3B) in PBS solution; (E) photocurrents of csUCNRs@TiO_2@CdS-modified ITO electrode in Tris−HCl solution (10 mM, pH 8.3) containing (a) nothing, (b) 2 mM TCEP, (c) 100 μM AA, (d) 100 μM AA and 2 mM TCEP, (e) the generated AA in the presence of 1 pM miRNA-133a, (f) the generated AA (the same as (e))and 2.0 mM TCEP; and (F) relationship between AA and photocurrent responses of csUCNRs@TiO_2@CdS-modified ITO electrodes (n = 3).

generated AA was directly introduced into the PEC detection pull containing TCEP to consume the photogenerated hole on the surface of csUCNRs@TiO_2@CdS for photocurrent measurement. TCEP, a reducing agent, could reduce the oxidation product DHA to regenerate AA through a chemical redox process, which further enhanced the photocurrent response.

The morphology was characterized by scanning electron microscopy (SEM). Figure 1A shows that the initial core $NaYF_4$:Yb,Tm nanorods stabilized by EDTA were rod-like hexagonal prisms with lengths from 300 to 600 nm and an average width of 100 nm. To reduce surface defects and improve up-conversion luminous efficiency, a $NaYF_4$ layer was elaborately designed and coated around the $NaYF_4$:Yb,Tm core as depicted in Figure 1B. The csUCNRs with a smoother surface showed a nearly 700 nm length and 100 nm width and illuminated brighter blue light under a 980 nm NIR laser (Figure S1B). Upon one-step growth of TiO_2, a majority of nanoparticles tightly coating on the surface of csUCNRs could be obviously observed, as shown in Figure 1C. Next, the CdS nanoparticles were in situ nucleated and grown onto the csUCNR shell. As depicted in Figure 1D, an increased amount of nanoparticles could be easily found, confirming the formation of CdS. The TiO_2 and CdS nanoparticles formed a heterostructure simultaneously and could be regarded as the third layer surrounding the csUCNRs. To further prove the successful fabrication of csUCNRs@TiO_2@CdS, energy-dispersive spectrometry (EDS) elemental mapping (Figure 1E) was performed and the results showed all the desired elements, Y, Yb, Tm, Ti, O, Cd, and S, in the composite.

The crystal structure was investigated by powder X-ray diffraction (Figure 2A). The diffraction peaks at 17.2, 30.1, 30.8, 43.5, 52.3, and 53.8° of csUCNRs were assigned to the (1 0 0), (1 1 0), (1 0 1), (2 0 1), (3 0 0), and (2 1 1) crystal planes, respectively, of standard hexagonal $NaYF_4$ (JCPDS No. 16-0334). These peaks could also be clearly observed after decoration of TiO_2 and CdS nanoparticles, indicating that the crystal structure of csUCNRs had not been altered. Furthermore, the newly emerging obvious peaks at 28.2 and 47.8° corresponded well to the lattice parameters of hexagonal CdS, which further confirmed the existence of CdS.

Subsequently, the chemical states of csUCNRs@TiO_2@CdS were characterized by X-ray photoelectron spectroscopy (XPS). All the expected elements were found in the full XPS spectra (Figure 2B). In the high-resolution XPS spectrum, the peaks at 464 and 458.5 eV demonstrated the formation of Ti^{4+} (Figure 2C). In addition, the binding energies at 531.45 and 529.4 eV were assigned to H—O and Ti—O band separately, illustrating the existence of O^{2-} (Figure 2D). Furthermore, the characteristic peaks of Cd 3d at 411.51 and 404.71 eV (Figure 2E) and S 2p at 161.45 and 159.35 eV proved the successful coordination of CdS (Figure 2F). Also, the peaks at 186.55 and 175, 172.7 eV belong to the Yb^{3+} and Tm^{3+}, respectively (Figure S2). All the aforementioned statistics confirmed the successful synthesis of core−shell−shell structured csUCNRs@TiO_2@CdS that functioned as the footstone to photocurrent detection.

Feasibility of the miRNA133a-Responsive NIR-Initiated PEC Biosensor. In the work, the Yb^{3+} and Tm^{3+}-doped csUCNRs were selected as harvesters to absorb the 980 nm NIR laser source and emit short wavelength light, which can be absorbed subsequently by the surface-wrapped UV/vis-responsive TiO_2@CdS shell to produce a photocurrent signal. The absorption and emission spectra were preliminarily tested, as shown in Figure 3A,B. The TiO_2 and CdS nanoparticles presented the absorption region from 270 to 420 nm with a

https://doi.org/10.1021/acs.analchem.1c02160
Anal. Chem. 2021, 93, 11251−11258

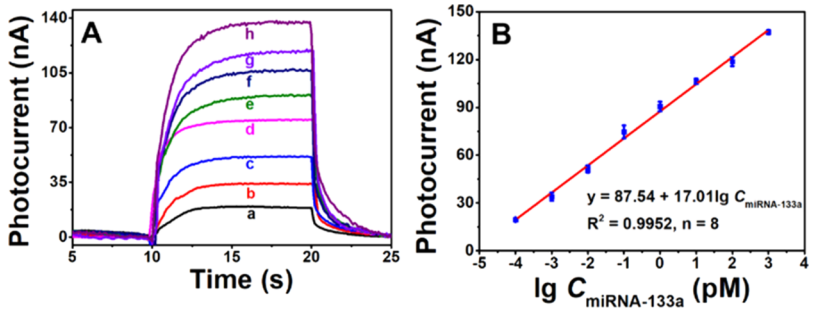

Figure 4. (A) Photocurrent of the csUCNRs@TiO_2@CdS-based PEC biosensor at different miRNA-133a concentrations: (a−h) 0.1 fM to 1 nM with the interval of an order of magnitude; and (B) corresponding calibration curve of the photocurrent towards target.

characteristic peak summit at 366 nm and 250 to 520 nm, respectively, on account of the respective band gap values of them (3.13 and 2.27 eV, Figure S3A). Meanwhile, the as-fabricated UCNRs, where Yb^{3+} with a relatively large absorption cross section acted as a sensitizer to absorb 980 nm NIR light and Tm^{3+} acted as an activator to provide various emissions, showed a few sharp emission peaks at 292, 346, 363, 453, and 479 nm as demonstrated in Figure 3B, originating from the $^1I_6 \rightarrow {}^3H_6$, $^1I_6 \rightarrow {}^3F_4$, $^1D_2 \rightarrow {}^3H_6$, $^1D_2 \rightarrow {}^3F_4$, and $^1G_4 \rightarrow {}^3H_6$ transitions of Tm^{3+}, respectively. Also, curve b in Figure 3B displayed higher upconversion luminescence intensity than the core alone, confirming the superiority of the core−shell structure of csUCNRs. Upon the modification of TiO_2 and CdS step by step, the fluorescence intensity descended as expected, indicating that the emissions of csUCNRs matched well with the absorption of the TiO_2@CdS shell. Then, the HCR process that could be triggered by miRNA-133a was verified by 10% native polyacrylamide gel electrophoresis (PAGE) (Figure 3C). A clear bright stripe with a low molecular weight could be observed in lanes 1 to 4, representing H1, H2, target RNA, and cDNA alone, respectively. Also, no obvious new stripes appeared in lane 5, mixing H1 and H2, and lane 6, mixing H1, H2, and cDNA. When miRNA-133a was introduced, a few new stripes with various high molecular weights appeared and formed a sliding zone. The results indicated that only miRNA-133a could initiate the HCR between H1 and H2.

To demonstrate the capability of csUCNRs@TiO_2@CdS as a photosensitive material and the role of AA and TCEP in signal amplification,[34] the PEC detection was implemented. As depicted in Figure 3D, the $NaYF_4$:Yb,Tm core (curve a) and csUCNR (curve b)-modified ITO electrodes showed a negligible photocurrent response due to the low background signal of the upconversion material. Meanwhile, the photocurrent of csUCNRs@TiO_2 (curve c)- and csUCNRs@TiO_2@CdS (curve d)-modified electrodes were increased to nearly 11 and 15 nA due to the effective electron transfer on the conduction band from CdS to TiO_2 under NIR irradiation as illustrated in Scheme 1, indicating that csUCNRs@TiO_2@CdS could be used for PEC detection.

Moreover, the photocurrent response was largely enhanced upon the introduction of AA and AA/TCEP, confirming that the holes on the valence bond of CdS were consumed by AA, which was in turn regenerated by TECP reduction as shown in Figure 3E (curves c and d). In addition, the TCEP alone (curve b) could not consume the holes on the surface of the electrode to enhance the photocurrent, further confirming the reducing agent function in the redox circle process. After that, the AA generated during the aforementioned miRNA-133a identification and HCR signal amplification process was transferred into the detection pull and obvious augmentation of photocurrent was observed in Figure 3E (curve e). When TCEP was also added, the photocurrent response rose again (Figure 3E, curve f). Figure 3F showed a linear relationship with the concentration of AA ranging from 10 to 100 μM, which makes it possible to quantitatively detect miRNA-133a. The results discussed above solidly validated the feasibility of the sensing method.

Optimization of Experimental Conditions. The effects of pH of the reaction solution, concentration of photoactive material, reaction time between miRNA-133a and cDNA, and HCR time on photocurrent performance were studied. As shown in Figure S4D, the photocurrent first increased and then went down with the pH ranging from 7.5 to 8.5, showing a maximum value at pH 8.3. With the increase of csUCNRs@TiO_2@CdS concentration, the photocurrent response rose rapidly and then reached a maximum at the concentration of 2.0 mg/mL followed by a slow descent in intensity. The increase in photocurrent response is due to the enhanced photoinduced carriers generated by the csUCNRs@TiO_2@CdS, while the decrease in photocurrent response is ascribed to the confinement of electron transfer from the csUCNRs@TiO_2@CdS to ITO for deposited thicker layers (Figure S4A). Thus, 2.0 mg mL^{-1} was recognized as the optimum concentration of csUCNRs@TiO_2@CdS. Furthermore, the incubation time between miRNA-133a and cDNA and HCR time were also studied. In addition, the variation tendency of photocurrent intensity elevated quickly initially and then reached a plateau. A 70 min miRNA-133a-cDNA incubation time and 100 min of HCR time were chosen as the suitable conditions, as confirmed from Figure S4B,C. Therefore, pH 8.3 of Tris−HCl solution, 2.0 mg/mL of csUCNRs@TiO_2@CdS, 70 min reaction time, and 100 min of HCR time were selected for the following experiments.

Analytical Performance of the miRNA133a-Responsive NIR-Initiated PEC Biosensor. Under the optimized conditions, the as-constructed biosensor was employed to quantitatively determine miRNA-133a with a sequence of concentrations from 0.1 fM to 1 nM under 980 nm irradiation. As depicted in Figure 4A, the photocurrent exhibited a superb linear relationship with the logarithmic concentration of miRNA-133a. The linear regression equation was $y = 87.54 + 17.01 \lg C_{\text{miRNA-133a}}$ (pM) with a satisfactory correlation coefficient (Figure 4B, $R^2 = 0.9952$). Also, the limit of detection (LOD) was calculated to be 36.12 aM (S/N = 3), which was comparable or even advantageous to the previous status owing to the immobilization-free strategy and double signal amplification (Table S2). The biosensing platform has

https://doi.org/10.1021/acs.analchem.1c02160
Anal. Chem. 2021, 93, 11251−11258

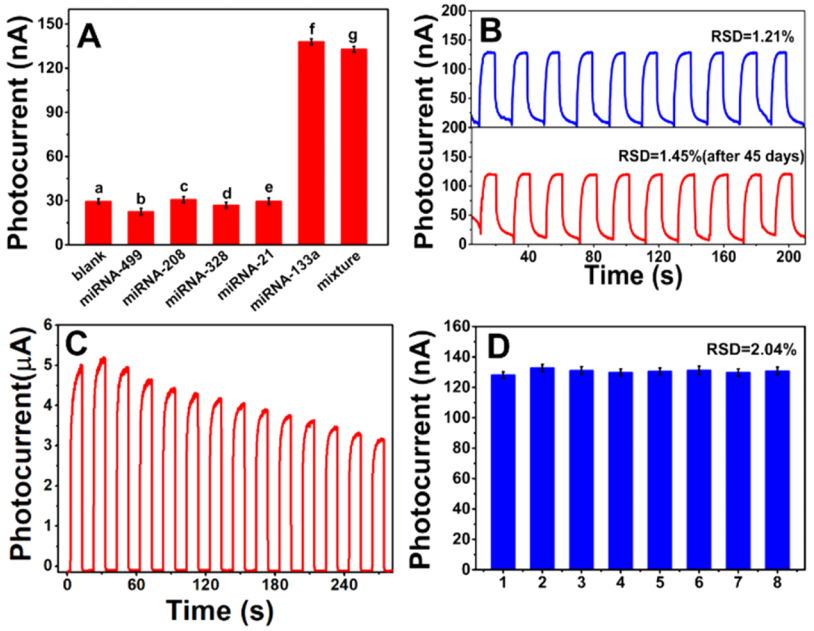

Figure 5. (A) Selectivity of the PEC sensor to 1 pM of (a) blank, (b) miRNA-499, (c) miRNA-208, (d) miRNA-328, and (e) miRNA-21, 100 fM of (f) miRNA-133a, and (g) the mixture of 1 pM interferences and 100 fM miRNA-133a; (B) stability of the PEC sensor toward miRNA-133a under 10 cycles of successive detection before (blue) and after 45 days (red); (C) photocurrent response of the PEC biosensor under 14 cycles of successive UV/vis light irradiation; and (D) reproducibility of this assay with eight independently prepared biosensors.

potential to satisfy the requirements for miRNA-133a detection with guaranteed sensitivity in a complex environment.

Selectivity, Stability, and Reproducibility of the NIR-Initiated PEC Biosensor. miRNA-499, miRNA-208, miRNA-328, and miRNA-21 (1 pM) as potential interferences were detected using the biosensor to demonstrate its specificity to miRNA-133a. The photocurrents of AMI-relevant interferences (lanes b−e) were near to that of the blank (lane a) and much lower than those of miRNA-133a (lane f) and the mixture (lane g) containing 1 pM of interferences and 100 fM of target miRNA-133a (Figure 5A), suggesting that only miRNA-133a could be recognized and open the hairpin structure of cDNA through complementary base pairing, which triggered the HCR amplification process and the production of AA. In addition, the stability and reproducibility were both crucial elements of the biosensor to determine its practicability. Figure 5B clearly displays that the photocurrent was steady enough during the 10 sequential and periodic cycles and the photocurrent was slightly lower than the original results even after storing for 45 days with corresponding relative standard deviations (RSD) of 1.21 and 1.21%. However, the photocurrent evoked by UV/vis light dropped gradually as shown in Figure 5C. All the outcomes demonstrated the excellent stability of the biosensor and the superiority of exertion of the NIR light source. Furthermore, we fabricated eight biosensors using the same synthetic method and all had good photocurrent performance with an interassay RSD of 2.04% (Figure 5D). All the consequences confirmed the excellent performance of the biosensor.

Analysis of Human Serum Samples. To verify the applicability of the csUCNR-based PEC biosensor in real samples, various concentrations (100 fM, 1pM, and 10 pM) of miRNA-133a were dissolved in 10% human serum and then were detected by the biosensor (Table S3). The determination of the recoveries was calculated based on the above linear regression equation. The recoveries were from 98.71 to 102.18%, and RSDs were from 0.68 to 1.95%. These appreciable results demonstrated that our designed csUCNR-based NIR-initiated PEC biosensor would have potential for application in the clinical detection of miRNA.

CONCLUSIONS

In conclusion, a NIR-initiated PEC biosensor based on csUCNRs@TiO_2@CdS was constructed for miRNA-133a detection in an immobilization-free manner with a double signal amplification strategy. The emissions of csUCNRs driven by 980 nm laser could be exactly absorbed by the adjacent TiO_2@CdS shell to generate photocurrent. The employment of NIR light exhibited excellent chemical and optical stability, low photobleaching, and phototoxicity in the detection process. Moreover, owing to the homogeneously detection of miRNA-133a with double amplification including a HCR and redox circle reaction in solution, the biosensor displayed guaranteed sensitivity and selectivity and further was applied in real human serum. Therefore, the csUCNR-based NIR-initiated PEC biosensor offers a new visual angle for PEC detection for other biomarkers in complicated conditions. Moreover, improving the luminous efficiency of the upconversion material through adjusting the local symmetry of the luminous center or sensitization of dyes or quantum dots can be a breakthrough in UCNP-based PEC platforms.

ASSOCIATED CONTENT

Supporting Information

The Supporting Information is available free of charge at https://pubs.acs.org/doi/10.1021/acs.analchem.1c02160.

Reagents and chemicals; oligonucleotide sequences used in the work; partial experimental section; fluorescence images of the $NaYF_4$:Yb,Tm core and csUCNRS; XPS of Y 3d, Yb 4d, and Tm 4d orbitals; binding energy of CdS and TiO_2; optimized detection conditions; comparison

https://doi.org/10.1021/acs.analchem.1c02160
Anal. Chem. 2021, 93, 11251−11258

of different biosensors; miRNA-133a detection in human serum (PDF)

AUTHOR INFORMATION

Corresponding Authors

Jing Zhang − *School of Chemistry and Chemical Engineering, University of Jinan, Jinan 250022, China*; Email: zhangjingdadi@126.com

Mei Yan − *School of Chemistry and Chemical Engineering, University of Jinan, Jinan 250022, China*; orcid.org/0000-0002-7509-4262; Email: chm_yanm@126.com

Authors

Mengjiao Hao − *School of Chemistry and Chemical Engineering, University of Jinan, Jinan 250022, China*

Pei Miao − *School of Chemistry and Chemical Engineering, University of Jinan, Jinan 250022, China*

Yan Wang − *School of Chemistry and Chemical Engineering, University of Jinan, Jinan 250022, China*

Wenshou Wang − *School of Chemistry and Chemical Engineering, University of Jinan, Jinan 250022, China*; orcid.org/0000-0003-2674-4203

Shenguang Ge − *Institute for Advanced Interdisciplinary Research, University of Jinan, Jinan 250022, China*; orcid.org/0000-0002-0537-6491

Xinyan Yu − *School of Water Conservancy and Environment, University of Jinan, Jinan 250022, China*

Xiao-Xiao Hu − *College of Life Sciences, Molecular Science and Biomedicine Laboratory (MBL), State Key Laboratory of Chemo/Bio-Sensing and Chemometrics, College of Chemistry and Chemical Engineering, Aptamer Engineering Center of Hunan Province, Hunan University, Changsha 410082, China*

Biyan Ding − *School of Materials Science and Engineering, Qilu University of Technology (Shandong Academy of Sciences), Jinan 250353, China*

Complete contact information is available at: https://pubs.acs.org/10.1021/acs.analchem.1c02160

Notes

The authors declare no competing financial interest.

ACKNOWLEDGMENTS

This work was financially supported by the National Natural Science Foundation of China (22007038, 31970692, 21675064), the Shandong Provincial Natural Science Foundation (ZR2020LFG009, ZR2018ZC0230), the Taishan Scholars Program (TSQN 20161036), the project of "20 items of University" of Jinan (2019GXRC055), the Case-by-Case Project for Top Outstanding Talents of Jinan, the Open Project of Chemistry Department of Qingdao University of Science and Technology (QUSTHX202008), and the Changsha Science and Technology Plan (kq2004009).

REFERENCES

(1) Shu, D.; Li, H.; Shu, Y.; Xiong, G.; Carson, W. E., III; Haque, F.; Xu, R.; Guo, P. *ACS Nano* **2015**, *9*, 9731−9740.

(2) Bartel, D. P. *Cell* **2004**, *116*, 281−297.

(3) Cheng, M.; Yang, J.; Zhao, X.; Zhang, E.; Zeng, Q.; Yu, Y.; Yang, L.; Wu, B.; Yi, G.; Mao, X.; Huang, K.; Dong, N.; Xie, M.; Limdi, N. A.; Prabhu, S. D.; Zhang, J.; Qin, G. *Nat. Commun.* **2019**, *10*, 959.

(4) Wang, G.-K.; Zhu, J. Q.; Zhang, J. T.; Li, Q.; Li, Y.; He, J.; Qin, Y.-W.; Jing, Q. *Eur. Heart J.* **2010**, *31*, 659−666.

(5) Wang, J.; Haghighatbin, M. A.; Shen, W.; Mi, L.; Cui, H. *Anal. Chem.* **2020**, *92*, 7062−7070.

(6) Wu, L.; Wang, Y.; Xu, X.; Liu, Y.; Lin, B.; Zhang, M.; Zhang, J.; Wan, S.; Yang, C.; Tan, W. *Chem. Rev.* **2021**, DOI: 10.1021/acs.chemrev.0c01140.

(7) Zhai, Y.; Liu, D.; Jiang, Y.; Chen, X.; Shao, L.; Li, J.; Sheng, K.; Zhang, X.; Song, H. *Sens. Actuators B Chem.* **2019**, *286*, 468−475.

(8) Zhao, C.; Zhang, L.; Wang, Q.; Zhang, L.; Zhu, P.; Yu, J.; Zhang, Y. *ACS Appl. Mater. Interfaces* **2021**, *13*, 20397−20404.

(9) Yang, H.; Wang, J.; Li, X.; Zhang, L.; Yu, H.; Zhang, L.; Ge, S.; Yu, J.; Zhang, Y. *ACS Appl. Mater. Interfaces* **2021**, *13*, 19793−19802.

(10) Pan, L.; Sun, S.; Zhang, A.; Jiang, K.; Zhang, L.; Dong, C.; Huang, Q.; Wu, A.; Lin, H. *Adv. Mater.* **2015**, *27*, 7782−7787.

(11) Victorious, A.; Saha, S.; Pandey, R.; Soleymani, L. *Angew. Chem., Int. Ed.* **2021**, *60*, 7316−7322.

(12) Wu, W.; Zhang, Z. *J. Mater. Chem. B* **2017**, *5*, 4883−4889.

(13) Shu, J.; Tang, D. *Anal. Chem.* **2020**, *92*, 363−377.

(14) Liu, X.; Zhao, Y.; Li, F. *Biosens. Bioelectron.* **2021**, *173*, 112832.

(15) Cui, L.; Hu, J.; Wang, M.; Li, C.c.; Zhang, C.y. *Anal. Chem.* **2019**, *91*, 1232−1236.

(16) Yang, L.; Yin, X.; An, B.; Li, F. *Anal. Chem.* **2021**, *93*, 1709−1716.

(17) Lai, J.; Zhang, Y.; Pasquale, N.; Lee, K.-B. *Angew. Chem., Int. Ed.* **2015**, *53*, 14419−14423.

(18) Zhang, F.; Braun, G. B.; Shi, Y.; Zhang, Y.; Sun, X.; Reich, N. O.; Zhao, D.; Stucky, G. *J. Am. Chem. Soc.* **2010**, *13*, 2850−2851.

(19) Zheng, F.; Wang, C.; Meng, T.; Zhang, Y.; Zhang, P.; Shen, Q.; Zhang, Y.; Zhang, J.; Li, J.; Min, Q.; Chen, J.; Zhu, J.-J. *ACS Nano* **2019**, *13*, 12577−12590.

(20) Hao, C.; Wu, X.; Sun, M.; Zhang, H.; Yuan, A.; Xu, L.; Xu, C.; Kuang, H. *J. Am. Chem. Soc.* **2019**, *141*, 19373−19378.

(21) Luo, Z.; Zhang, L.; Zeng, R.; Su, L.; Tang, D. *Anal. Chem.* **2018**, *90*, 9568−9575.

(22) Ravetz, B. D.; Pun, A. B.; Churchill, E. M.; Congreve, D. N.; Rovis, T.; Campos, L. M. *Nature* **2019**, *570*, 343−346.

(23) Wang, F.; Liu, X. *J. Am. Chem. Soc.* **2008**, *130*, 5642−5643.

(24) Li, H.; Wang, X.; Ohulchanskyy, T. Y.; Chen, G. *Adv. Mater.* **2021**, *33*, 2000678.

(25) Tou, M.; Mei, Y.; Bai, S.; Luo, Z.; Zhang, Y.; Li, Z. *Nanoscale* **2016**, *8*, 553−562.

(26) Yang, Y.; Shao, Q.; Deng, R.; Wang, C.; Teng, X.; Cheng, K.; Cheng, Z.; Huang, L.; Liu, Z.; Liu, X.; Xing, B. *Angew. Chem., Int. Ed.* **2012**, *51*, 3125−3129.

(27) Fang, Y.; Li, Y.; Li, Y.; He, R.; Zhang, Y.; Zhang, X.; Liu, Y.; Ju, H. *Anal. Chem.* **2021**, 7258.

(28) Mi, Y.; Zhao, J.; Chu, H.; Li, Z.; Yu, M.; Li, L. *Multiplexed Molecular Imaging. Anal. Chem.* **2021**, *93*, 2500−2509.

(29) Jia, H.; Li, D.; Zhang, D.; Dong, Y.; Ma, S.; Zhou, M.; Di, W.; Qin, W. *ACS Appl. Mater. Interfaces* **2021**, *13*, 4402−4409.

(30) Cen, Y.; Deng, W. J.; Yang, Y.; Yu, R. Q.; Chu, X. *Anal. Chem.* **2017**, *89*, 10321−10328.

(31) Song, X.; Li, S.; Guo, H.; You, W.; Shang, X.; Li, R.; Tu, D.; Zheng, W.; Chen, Z.; Yang, H.; Chen, X. *Angew. Chem., Int. Ed.* **2019**, *131*, 19157−19162.

(32) Lv, S.; Zhang, K.; Zhu, L.; Tang, D. *Anal. Chem.* **2020**, *92*, 1470−1476.

(33) Qiu, Z.; Shu, J.; Liu, J.; Tang, D. *Anal. Chem.* **2019**, *91*, 1260−1268.

(34) Ye, X.; Wang, X.; Kong, Y.; Dai, M.; Han, D.; Liu, Z. *Angew. Chem., Int. Ed.* **2021**, *60*, 11774−11778.

(35) Gao, J.; Yao, X.; Chen, Y.; Gao, Z.; Zhang, J. *Anal. Chem.* **2020**, *93*, 677−682.

(36) Wu, J.; Lv, W.; Yang, Q.; Li, H.; Li, F. *Biosens. Bioelectron.* **2021**, *171*, 112707.

(37) Wu, J.; Yang, Q.; Li, Q.; Li, H.; Li, F. *Anal. Chem.* **2021**, *93*, 4084−4091.

(38) Yin, X.; Hou, T.; Huang, B.; Yang, L.; Li, F. *Chem. Commun.* **2019**, *55*, 13705−13708.

(39) Tan, Y.; Wei, X.; Zhang, Y.; Wang, P.; Qiu, B.; Guo, L.; Lin, Z.; Yang, H.-H. *Anal. Chem.* **2015**, *87*, 11826−11831.
(40) Li, Y.; Yu, F.; Chen, S.; Zhang, N.; Wang, H.; Zhao, Q. *Anal. Chem.* **2021**, *93*, 4794−4799.
(41) Qiu, Z.; Shu, J.; Tang, D. *Anal. Chem.* **2018**, *90*, 1021−1028.
(42) Mo, F.; Han, M.; Weng, X.; Zhang, Y.; Li, J.; Li, H. *Anal. Chem.* **2021**, *93*, 1764−1770.
(43) Kumar, A.; Reddy, K. L.; Kumar, S.; Kumar, A.; Sharma, V.; Krishnan, V. *ACS Appl. Mater. Interfaces* **2018**, *10*, 15565−15581.
(44) Sun, J.; Song, L.; Fan, Y.; Tian, L.; Luan, S.; Niu, S.; Ren, L.; Ming, W.; Zhao, J. *ACS Appl. Mater. Interfaces* **2019**, *11*, 26581−26589.
(45) Wang, H.; Chen, S.; Li, L.; Jiang, S. *Langmuir* **2005**, *21*, 2633−2636.
(46) Wang, S.; Zhao, J.; Zhang, Y.; Yan, M.; Zhang, L.; Ge, S.; Yu, J. *Biosens. Bioelectron.* **2019**, *139*, 111325.

https://doi.org/10.1021/acs.analchem.1c02160
Anal. Chem. 2021, 93, 11251−11258